# Mass dependence of critical behavior in nucleus-nucleus collisions

T. Li, W. Bauer, D. Craig, E. Gualtieri, S. Hannuschke, R. Pak, A. M. Vander Molen, G. D. Westfall, J. S. Winfield, J. Yee, and S. J. Yennello
*National Superconducting Cyclotron Laboratory and Department of Physics and Astronomy, Michigan State University, East Lansing, Michigan 48824*

R. Lacey
*Department of Chemistry, State University of New York at Stony Brook, Stony Brook, New York 11794*

A. Nadasen
*Department of Physics, University of Michigan at Dearborn, Dearborn, Michigan 48128*

R. S. Tickle
*Department of Physics, University of Michigan, Ann Arbor, Michigan 48109*

E. Norbeck
*Department of Physics and Astronomy, University of Iowa, Iowa City, Iowa 52242*
(Received 12 April 1993)

The $Z$ distributions of fragments emitted from central collisions of $^{40}$Ar + $^{45}$Sc at beam energies from 15 to 115 MeV/nucleon have been fitted to power laws $\sigma(Z) \propto Z^{-\lambda}$. The $\lambda$ parameter reaches a minimum at a beam energy of $23.9 \pm 0.7$ MeV/nucleon. A percolation model calculation reproduces the observed $Z$ distributions for all beam energies, using the mean excitation energy as extracted from proton kinetic energy spectra. We extract the critical value of the deposited excitation energy for our system and make predictions for the dependence of this quantity on the size of the fragmenting system.

PACS number(s): 25.70.Pq

Central collisions of heavy ions at intermediate beam energies from 10 MeV/nucleon to several hundred MeV/nucleon go through two stages: an initial compression stage and a final expansion stage. In these reactions the compression can create nuclear matter density as high as twice the normal nuclear density and equilibrated matter with mean excitation energy of several tens of MeV per nucleon. Therefore intermediate energy heavy- ion reactions may provide information on the thermodynamic properties of nuclear matter, i.e., the nuclear matter equation of state (EOS), if finite-size effects of the reaction system are taken into account. From consideration of the long-range attractive mean-field interaction and short-range repulsive nucleon-nucleon interactions in nuclear reactions, a liquid-gas phase transition has been predicted by comparing the nuclear matter EOS with the Van der Waals EOS [1–6]. This phase transition is of first order, terminating in a second-order phase transition at the critical point. The cluster size distribution at the critical point is given by $\sigma(A) \propto A^{-\tau}$, where $\tau$ is a critical exponent with a value characteristic of the universality class of the phase transition, and $A$ is the cluster size. It has been shown [7–9] that for small-size systems in the vicinity of the critical point, the clusters' size distribution can be fitted by a power law with apparent exponent $\lambda$, which has a minimum, $\lambda_{\min} = \tau$, at the critical point.

The previously measured inclusive cluster distributions of proton-induced reaction [10,11] do exhibit power-law features and indicate a critical behavior. However, these measurements summed over different impact parameters with different excitation energies. To obtain an unambiguous signature of the phase transition, well-characterized central collisions with well-defined excitation-energy deposition into the system need to be measured and the finite-size effects have to be addressed.

We chose a nearly symmetric system, $^{40}$Ar + $^{45}$Sc, to suppress projectile and target spectators in central collisions. The experiment was done with the Michigan State University $4\pi$ Array [12] with Bragg curve spectrometers [13]. Beam energies of 15, 25, 35, 45, 65, 75, 85, 95, 105, and 115 MeV/nucleon were used to cover the excitation-energy region for which most of the theories predict the occurrence of the second-order phase transition [1,3,8,14]. The correction for detector acceptance and centrality selection has been discussed previously [15].

To estimate the finite-size effect, a bond-breaking percolation calculation [7,14,16–27] is performed. The bond-breaking percolation model assumes that each nucleon is "linked" with its nearest neighbors by potential bonds. Each bond can absorb a maximum energy, called the bond-breaking energy, $E_b$, and has a probability, $P_b$, to break. Such simulations have allowed the fitting of $P_b$ to experimental data for $Z$ distributions from heavy-ion reactions [27].

In the present work, we assume that the energy distributed into each bond, $\epsilon_b$, can be described by a Boltzmann distribution with a mean energy $\langle \epsilon_b \rangle$. Each site of the lattice has an average of $\alpha$ bonds. The average excitation energy deposited per site is $\langle E_s \rangle = \alpha \langle \epsilon_b \rangle$, and the

 

binding energy per nucleon of the initial nuclear system is $B = \alpha E_b$. When the system expands, any bond which has an energy greater than $E_b$ will break. Therefore the bond-breaking probability is

$$P_b = \int_{E_b}^{\infty} \sqrt{\epsilon_b} e^{-\epsilon_b/t_b} d\epsilon_b \Big/ \int_0^{\infty} \sqrt{\epsilon_b} e^{-\epsilon_b/t_b} d\epsilon_b$$
$$= \int_B^{\infty} \sqrt{E_s} e^{-E_s/T_s} dE_s \Big/ \int_0^{\infty} \sqrt{E_s} e^{-E_s/T_s} dE_s,$$

where $t_b = \frac{2}{3}\langle \epsilon_b \rangle$ and $T_s = \alpha t_b = \frac{2\alpha}{3}\langle \epsilon_b \rangle = \frac{2}{3}\langle E_s \rangle$ are slope parameters. We note that the bond-breaking probability $P_b$ calculated by Eq. (1) is independent of $\alpha$, therefore the calculation is independent of the lattice structure.

We also note in passing that this approach is consistent with the introduction of the mean coordination $\langle c \rangle \equiv \alpha \cdot (1 - p_b)$. It can be shown that, for example, the mean multiplicity of clusters per lattice site is very different for different lattice structures when plotted as a function of $p_b$. But there is hardly a difference between different lattice structures, if one plots the same quantity against $\langle c \rangle$. This is again an example of the independence of the physical quantities from the lattice structure, once the trivial $\alpha$ dependence is removed.

It should also be pointed out here that the relevant degrees of freedom in the above equation are *not* the bonds (the number of which is somewhat arbitrary and dependent on the specific lattice structure chosen), but the sites (i.e., nucleons) whose number is fixed. We chose to use the classical Boltzmann statistics, but at the excitation energies relevant here and in the limit of large number of nucleons, this classical approximation should be sufficient. One can also obtain a formula similar to the one above by constructing an analogy between the bond percolation model and the Ising model of ferromagnets [28–30].

By fitting the proton kinetic-energy spectra with a single moving Boltzmann source [31–33], we obtain the slope parameters $T_s$ for each beam energy. The initial size of the lattice is assumed to be given by the fireball geometry for an overlap region of projectile and target with impact parameter of 0.25 $b_{\max}$, where $b_{\max}$ is the sum of the radii of the projectile and the target nuclei. This cutoff in impact parameter was chosen in order to approximate the experimental centrality trigger. It should be pointed out here that the mean excitation energy per nucleon is dependent on the impact parameter for asymmetric systems, but independent for symmetric systems. This is because the projectile mass fraction in the overlap zone is always 1/2 in the symmetric case. Therefore

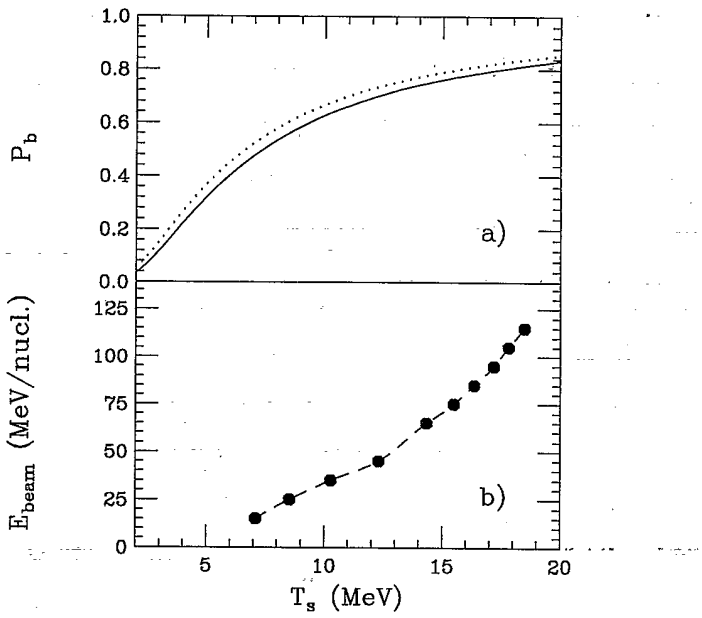


FIG. 1. (a) Bond-breaking probability $P_b$ vs slope parameters $T_s$ calculated using Eq. (1) with a binding energy of 7 MeV/nucleon (dotted curve) and 7.8 MeV/nucleon (solid curve). (b) Slope parameters of proton kinetic-energy spectra for beam energies from 15 to 115 MeV/nucleon obtained by a single moving relativistic Boltzmann source fit to the proton kinetic-energy spectra in the laboratory frame.

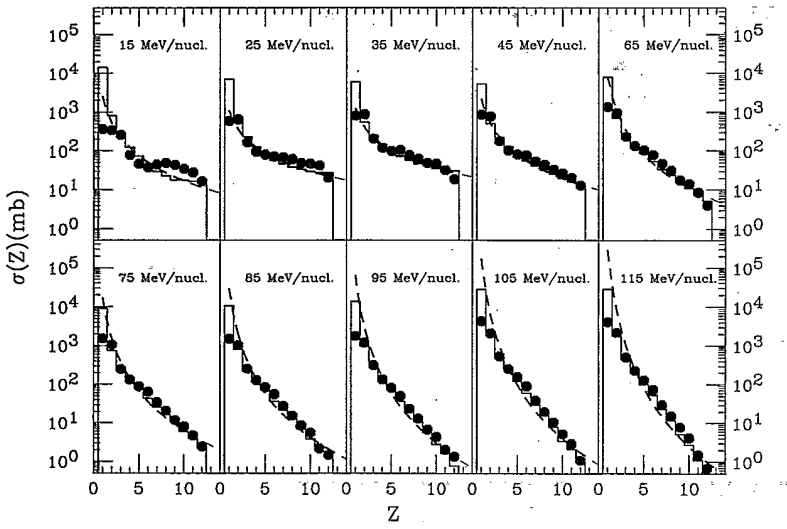


FIG. 2. $Z$ distributions of both experimental data and percolation calculations of $^{40}$Ar + $^{45}$Sc at 15 to 115 MeV/nucleon. The solid circles are $Z$ distributions corrected for detector acceptance from central collisions of $^{40}$Ar + $^{45}$Sc, and the histograms are percolation calculations with an initial lattice size of 68 and a binding energy of 7.8 MeV/nucleon. The percolation calculations are normalized to experimental data for $3 \leq Z \leq 12$. The dashed curves are power-law fits to the percolation calculations.

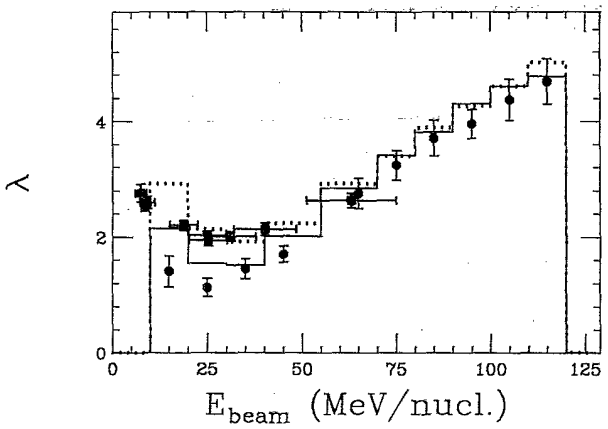


FIG. 3. Comparison of power-law fitting parameters, $\lambda$, to the percolation calculations with experimental results. The solid circles are the power-law $[\sigma(Z) \sim Z^{-\lambda}]$ fit to the experimental data of Ar + Sc from 15 to 115 MeV/nucleon, and the open squares are GSI data of Au + C, Al, and Cu at 600 MeV/nucleon [34]. The solid histogram is the power-law fit to the percolation calculations with a lattice size of 68 calculated from fireball geometry and a binding energy of 7.8 MeV/nucleon. The dashed histogram is the percolation calculation for a lattice size of 150 with a binding energy of 7.0 MeV/nucleon.

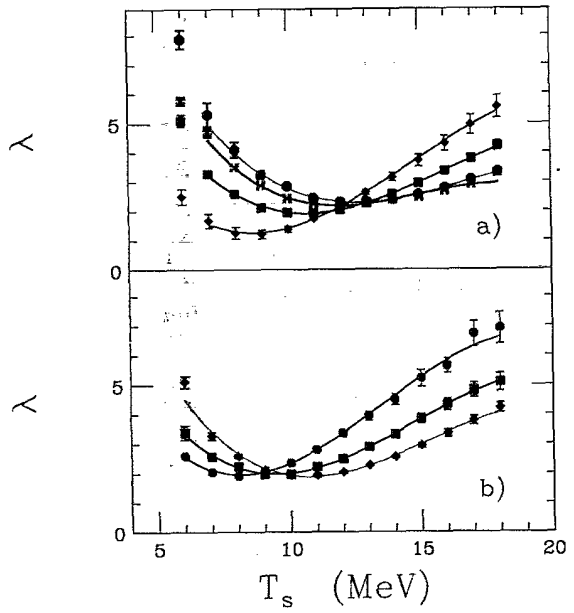


FIG. 4. (a) The apparent exponent of the power-law fits, $\lambda$, as a function of the slope parameter $T_s$ for different initial lattice size. The solid diamonds are for size 50, the squares are for size 100, the crosses are for size 200, and the solid circles are for size 500. The solid curves are four-term polynomial fits to the points. (b) The power-law parameter as a function of $T_s$ with different binding energies. The lattice size is 100 and the binding energies are 6 MeV/nucleon (solid circles), 7 MeV/nucleon (solid squares), and 8 MeV/nucleon (solid diamonds). All error bars are statistical.

our assumption of impact-parameter independent excitation energy per nucleon of the participant zone should be valid in good approximation.

Therefore we used an initial cubic lattice of 68 sites with the bond-breaking probabilities calculated by Eq. (1), using the slope parameters of protons and a binding energy of 7.8 MeV/nucleon. The binding energy was used as a fitting parameter. We also compare this calculation to fragmentation data of 600 MeV/nucleon Au + C, Al, and C in Ref. [34]. We convert the excitation energies calculated by Ref. [34] to beam energies of a symmetric system (projectile and target have equal masses) assuming a total inelastic collision. Then the same beam energy as $^{40}$Ar + $^{45}$Sc and proton slope parameters are used with an initial lattice of 150 sites to reproduce the Au + C, Al, and Cu data. For Au + C, Al, and Cu, a 7.0 MeV/nucleon binding energy was found.

Figure 1(a) shows the bond-breaking probability vs slope parameter $T_s$ calculated by Eq. (1) with $B = 7.0$ MeV/nucleon (dotted curve) and $B = 7.8$ MeV/nucleon (solid curve). The slope parameters for each beam energy are shown in Fig. 1(b). Figure 2 shows the experimental $Z$ distributions corrected for detector acceptance from central collisions of $^{40}$Ar + $^{45}$Sc at beam energies from 15 to 115 MeV/nucleon (solid circle), compared to our percolation calculation (histogram). The dashed curve is the percolation calculation fitted to a power-law distribution, $\sigma(Z) \propto Z^{-\lambda}$. The percolation results are normalized to the experimental data for $3 \leq Z \leq 12$. The apparent exponent of the power law, $\lambda$, vs beam energy is shown in Fig. 3. The solid circles are the power law fits to the experimental data of $^{40}$Ar + $^{45}$Sc, and the solid histogram is the percolation calculation with 68 sites and a binding energy of 7.8 MeV/nucleon. The open squares are GSI data of Au + C, Al, and Cu at 600 MeV/nucleon [34], and the dotted histogram is the percolation calculation with 150 sites and 7.0 MeV/nucleon binding energy. The equivalent beam energy on the plot for the GSI data is obtained by converting the excitation energy calculated by Ref. [34] to a symmetric system assuming a total inelastic collision. To obtain the critical exponent, $\tau$, we fit the $\lambda$ vs $E_{\text{beam}}$ with a four term polynomial. For $^{40}$Ar + $^{45}$Sc, we get $\tau = 1.21 \pm 0.01$ at a beam energy of 23.9±0.7 MeV/nucleon. The percolation calculation with 68 sites and a binding energy of 7.8 MeV/nucleon gives $\tau = 1.5 \pm 0.1$ at a beam energy of $28 \pm 0.4$ MeV/nucleon. For GSI data of Au + C, Al, and Cu, we get $\tau = 2.0 \pm 0.01$ at a beam energy of $29 \pm 0.2$ MeV/nucleon. The percolation calculation with 150 sites and a binding energy of 7.0 MeV/nucleon gives $\tau = 1.98 \pm 0.03$ at a beam energy of $32.7 \pm 0.1$ MeV/nucleon. All errors are statistical.

In order to estimate the finite size effects and to obtain the critical excitation energy for infinite nuclear matter, we performed percolation calculations using a binding energy of 8 MeV/nucleon for different lattice sizes, ranging from 50 sites to 800 sites, and for slope parameters $T_s$ ranging from 5 MeV to 19 MeV. The critical excitation energy increases when the lattice size increases. Above 400 sites, the critical value for the slope parameter converges to $13.1 \pm 0.6$ MeV. This value can be compared with the theoretical calculation of 15.3 MeV given

by Ref. [1]. In Fig. 4(a), we plot the $\lambda$ parameter vs slope parameter $T_s$ for different lattice sizes. The solid curves are four-term polynomial fits for $T_s$ of 7 MeV to 19 MeV, made in order to extract the critical value. The diamonds are for size 50, squares are for size 100, crosses for size 200, and circles for size 500. For size 800 (not shown in the figure), the points are almost coincident with size 500, which indicates that the critical value of $T_s$ approaches an asymptotic limit at large size. Also, for 100 sites, we performed calculations for different binding energy to illustrate the sensitivity of the critical point with the binding energy. Figure 4(b) shows the calculation for $B = 6$ MeV/nucleon (solid circles), $B = 7$ MeV/nucleon (solid squares), and $B = 8$ MeV/nucleon (solid diamonds). All error bars in the figures are statistical. Figure 5(a) shows the critical value of slope parameter $T_c = T_s(\tau)$, extracted from the polynomial fits vs the size of the lattice. Figure 5(b) shows the critical exponent $\tau$ as a function of the lattice size. It approaches a limit of $2.3 \pm 0.2$ at a large size.

In conclusion, the $Z$ distributions of $^{40}$Ar + $^{45}$Sc have been measured, and power-law fits show a minimum of the apparent exponent $\lambda$ of $1.21 \pm 0.01$ at $23.9 \pm 0.7$ MeV/nucleon beam energy corresponding to a slope parameter of $T_s = 8.4 \pm 0.3$ MeV. The percolation calculation, using the binding energy as an adjustable parameter and proton kinetic energy slope parameters as input, reproduces both the experimental data of Ar + Sc and Au + C, Al, and Cu. The finite-size effect is estimated by increasing the initial lattice size of the percolation calculation. The critical value of $T_s$ approaches an asymptotic limit of $13.1 \pm 0.6$ MeV for a binding energy of 8 MeV/nucleon.

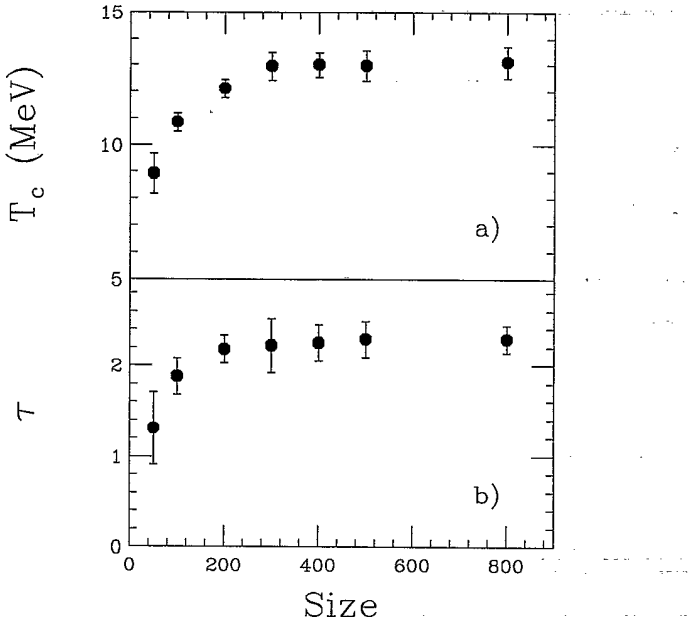


FIG. 5. The size dependence of the critical value of slope parameter $T_c = T_s(\tau)$ and the critical exponent $\tau$. (a) The critical slope parameter $T_c$ with different initial lattice size. (b) The critical power-law exponent $\tau$ as function of initial lattice size.

## ACKNOWLEDGMENTS

This work was supported in part by the National Science Foundation under Grant No. PHY-89-13815 and No. PHY-90-17077. W. Bauer acknowledges partial support from an NSF Presidential Faculty Fellow award.

[1] D. H. Boal and A. L. Goodman, Phys. Rev. C **33**, 1690 (1986).
[2] A. L. Goodman, J. I. Kapusta, and A. Z. Mekjian, Phys. Rev. C **30**, 851 (1984).
[3] J. Kapusta, Phys. Rev. C **29**, 1735 (1984).
[4] H. R. Jaqaman, A. Z. Mekjian, and L. Zamick, Phys. Rev. C **29**, 2067 (1984).
[5] J. Hüfner, Phys. Rep. **125**, 131 (1985).
[6] L. P. Csernai and J.I. Kapusta, Phys. Rep. **131**, 223 (1986).
[7] W. Bauer, D. R. Dean, U. Mosel, and U. Post, Phys. Lett. **150B**, 53 (1985).
[8] A. D. Panagiotou, M. W. Curtin, H. Toki, D. K. Scott, and P. J. Siemens, Phys. Rev. Lett. **52**, 496 (1984).
[9] M. E. Fisher, Physics **3**, 255 (1967).
[10] N. T. Porile, A. J. Bujak, D. D. Carmony, Y. H. Chung, L. J. Gutay, A. S. Hirsch, M. Mahi, G. L. Paderewski, T. C. Sangster, R. P. Scharenberg, and B. C. Stringfellow, Phys. Rev. C **39**, 1914 (1989).
[11] A. S. Hirsch, A. Bujak, J. E. Finn, L. J. Gutay, R. W. Minich, N. T. Porile, R. P. Scharenberg, and B. C. Stringfellow, Phys. Rev. C **29**, 508 (1984).
[12] G. D. Westfall, J. E. Yurkon, J. Van der Plicht, Z. M. Koenig, B. V. Jacak, R. Fox, G. M. Crawley, M. R. Maier, and B. E. Hasselquist, Nucl. Instrum. Methods **A238**, 347 (1985).
[13] D. Cebra, S. Howden, J. Karn, D. Kataria, M. Maier, A. Nadasen, C. A. Ogilvie, N. Stone, D. Swan, A. M. Vander Molen, W. K. Wilson, J. S. Winfield, J. Yurkon, G. D. Westfall, and E. Norbeck, Nucl. Instrum. Methods **A300**, 518 (1991).
[14] W. Bauer, Phys. Rev. C **38**, 1297 (1988).
[15] T. Li, W. Bauer, D. Craig, M. Cronqvist, E. Gualtieri, S. Hannuschke, R. Lacey, W. J. Llope, T. Reposeur, A. M. Vander Molen, G. D. Westfall, W. K. Wilson, J. S. Winfield, J. Yee, S. J. Yennello, A. Nadasen, R. S. Tickle, and E. Norbeck, Phys. Rev. Lett. **70**, 1924 (1993).
[16] D. Stauffer, Phys. Rep. **54**, 1 (1979).
[17] X. Campi, J. Phys. A **19**, L917 (1986).
[18] W. Bauer, U. Post, D.R. Dean, and U. Mosel, Nucl. Phys. **A452**, 699 (1986).
[19] T.S. Biro, J. Knoll, and J. Richert, Nucl. Phys. **A459**, 692 (1986).
[20] H. W. Barz, J. P. Bondorf, R. Donangelo, and H. Schulz, Phys. Lett **169B**, 318 (1986).
[21] J. Desbois, Nucl. Phys. **A466**, 724 (1987).
[22] X. Campi, Phys. Lett. B **208**, 351 (1988).
[23] Y. D. Kim, M. B. Tsang, C. K. Gelbke, W. G. Lynch, N. Carlin, Z. Chen, R. Fox, W. G. Gong, T. Murakami, T. K. Nayak, R. M. Ronnigen, H. M. Xu, F. Zhu, W. Bauer, L. G. Sobotka, D. Stracener, D. G. Sarantites, Z. Majka, V. Abenante, and H. Griffin, Phys. Rev. Lett. **63**, 494

(1989).
[24] X. Campi, Nucl. Phys. **A495**, 259c (1989).
[25] J. Richert and P. Wagner, Nucl. Phys. **A517**, 399 (1990).
[26] L. Phair, W. Bauer, D. R. Bowman, N. Carlin, R. T. de Souza, C. K. Gelbke, W. G. Gong, Y. D. Kim, M. A. Lisa, W. G. Lynch, G. F. Peaslee, M. B. Tsang, C. Williams, F. Zhu, N. Colonna, K. Hanold, M. A. McMahan, G. J. Wozniak, and L. G. Moretto, Phys. Lett. B **285**, 10 (1992).
[27] X. Campi and H. Krivine, Nucl. Phys. **A545**, 161c (1992).
[28] A. Coniglio, H. E. Stanley, and W. Klein, Phys. Rev. Lett. **42**, 518 (1979).
[29] D. W. Herrmann and D. Stauffer, Z. Phys. B **44**, 339 (1981).
[30] K. Binder and D. Stauffer, in *Application of Monte-Carlo Methods in Statistical Physics*, edited by K. Binder (Springer, Heidelberg, 1984), p. 241.
[31] G. D. Westfall, J. Gosset, P. J. Johansen, A. M. Poskanzer, W. G. Meyer, H. H. Gutbrod, A. Sandoval, and R. Stock, Phys. Rev. Lett. **37**, 1202 (1976).
[32] G. D. Westfall, B. V. Jacak, N. Anantaraman, M. W. Curtin, G. M. Crawley, C. K. Gelbke, B. Hasselquist, W. G. Lynch, D. K. Scott, B. M. Tsang, M. J. Murphy, T. J. M. Symons, R. Legrain, and T. J. Majors, Phys. Lett. **116B**, 118 (1982).
[33] B. V. Jacak, G. D. Westfall, G. M. Crawley, D. Fox, C. K. Gelbke, L. H. Harwood, B. E. Hasselquist, W. G. Lynch, D. K. Scott, H. Stöcker, M. B. Tsang, and G. Buchwald, Phys. Rev. C **35**, 1751 (1987).
[34] C. A. Ogilvie, J. C. Adloff, M. Begemann-Blaich, P. Bouissou, J. Hubele, G. Imme, I. Iori, P. Kreutz, G. J. Kunde, S. Leray, V. Lindenstruth, Z. Liu, U. Lynen, R. J. Meijer, U. Milkau, W. F. J. Müller, C. Ngô, J. Pochodzalla, G. Raciti, G. Rudolf, H. Sann, A. Schüttauf, W. Seidel, L. Stuttge, W. Trautmann, and A. Tucholski, Phys. Rev. Lett. **67**, 1214 (1991).